Transition Met Chem (2015) 40:555–564
DOI 10.1007/s11243-015-9948-8

Three- and four-coordinate Ag(I) complexes of crotonate and bis(benzimidazole)-2-oxapropane ligands: syntheses, crystal structures, DNA-binding studies and antioxidant activities

Huilu Wu[1] · Fei Wang[1] · Furong Shi[1] · Zaihui Yang[1] · Han Zhang[1] · Hongping Peng[1]

Received: 16 January 2015 / Accepted: 18 May 2015 / Published online: 29 May 2015

Abstract Two V-shaped ligands, namely 1,3-bis(1-ethylbenzimidazol-2-yl)-2-oxapropane (etobb) and 1,3-bis(1-benzylbenzimidazol-2-yl)-2-oxapropane (bobb), have been prepared. Reaction of these ligands with $AgNO_3$ and sodium crotonate under in the dark afforded the complexes, $[Ag(etobb)_2](crotonate)\cdot C_2H_5OH\cdot 2(CH_3CN)\cdot 2(H_2O)$ **1** and [Ag(crotonate)(bobb)] **2**. Both complexes have been characterized by physicochemical and spectroscopic methods and also by X-ray single-crystal diffraction. The coordination environment of complex **1** can be described as distorted tetrahedral, while complex **2** has as a trigonal planar geometry. The DNA-binding properties of these complexes have been investigated by fluorescence, electronic absorption and viscosity measurements. The experimental results suggest that they bind to DNA by an intercalation mode. Complex **2** also exhibits excellent hydroxyl radical scavenging activity.

Introduction

The rational design and synthesis of coordination frameworks have attracted much attention for their fascinating structures [1–3], as well as their potential uses as functional materials [4–7]. The selection of appropriate ligands as building blocks is usually a key factor in controlling the structures of such complexes [8–10]. Benzimidazole derivatives are important constituents in many pharmacologically, catalytically and biologically active compounds and therefore correspond to significant synthetic targets [11–13]. Compared with other heterocyclic N-donor ligands, bis-benzimidazole ligands have some distinctive structural characteristics. The benzimidazole ring has a larger conjugated π-system; therefore, π–π stacking interactions may play important roles in their complexes. The compounds of Ag(I) with multidentate N-donor ligands have attracted interest for a number of reasons. The absence of crystal field stabilization for the d^{10} monovalent silver cation, coupled with its ability to tolerate a wide range of coordination geometries (with coordination numbers spanning 2–7), leads to considerable variation in the geometry and connectivity of the networks that can be formed when Ag(I) centers act as connectors [14, 15]. Their various biological applications have also attracted attention [16].

In this work, two new silver complexes have been synthesized through the structural variation of flexible N-donor ligands. The DNA-binding properties and antioxidant activities of the complexes were investigated.

Experimental

C, H and N elemental analyses were determined using a Carlo Erba 1106 elemental analyzer. Electrolytic conductance measurements were made with a DDS-11A-type conductivity bridge using 10^{-3} mol L^{-1} solutions in DMF at room temperature. IR spectra were recorded in the 4000–400 cm^{-1} region with a Nicolet FT-VERTEX 70 spectrometer using KBr pellets. Electronic spectra were recorded on a Lab-Tech UV Bluestar spectrophotometer. ^1H NMR spectra were recorded on a Varian VR300 MHz spectrometer with TMS as an internal standard. Fluorescence spectra were recorded on a Perkin Elmer LS-45 spectrofluorophotometer. The antioxidant activities against

✉ Huilu Wu
wuhuilu@163.com

[1] School of Chemical and Biological Engineering, Lanzhou Jiaotong University, Lanzhou 730070, Gansu, People's Republic of China

hydroxyl and superoxide anion radicals were measured in a water bath with a Spectrumlab 722sp spectrophotometer.

Calf thymus DNA (CT-DNA) and ethidium bromide (EB) were obtained from Sigma-Aldrich. All chemicals and solvents were reagent grade and used without further purification. Tris–HCl buffer, Na_2HPO_4–NaH_2PO_4 buffer and EDTA-Fe(II) solution were prepared using double-distilled water. Stock solutions of the complexes were prepared in DMF at 3×10^{-3} mol L^{-1}. The experiments involving the interactions of the free ligands and complexes with CT-DNA were carried out in double-distilled buffered water containing 5 mM Tris and 50 mM NaCl and adjusted to pH 7.2 with hydrochloric acid. A solution of CT-DNA gave a ratio of UV absorbance at 260 and 280 nm of about 1.8–1.9, indicating that the CT-DNA was sufficiently free of protein [17]. The CT-DNA concentration per nucleotide was determined spectrophotometrically by employing an extinction coefficient of 6600 M^{-1} cm^{-1} at 260 nm [18]. Viscosity experiments were conducted using an Ubbelodhe viscometer, immersed in a water bath maintained at 25.0 ± 0.1 °C. Titrations were performed for the complex (3 μM), and each compound was introduced into CT-DNA solution (50 μM) present in the viscometer. Data were analyzed as $(\eta/\eta_0)^{1/3}$ versus the ratio of the concentration of the compound to CT-DNA, where η is the viscosity of CT-DNA in the presence of the compound and η_0 is the viscosity of CT-DNA alone.

Hydroxyl radicals were generated in aqueous media through the Fenton-type reaction [19]. The reaction mixtures (3 mL) contained 1 mL of 40 μg mL^{-1} aqueous safranin, 1 mL of 1.0 mmol aqueous EDTA-Fe(II), 1 mL of 3 % aqueous H_2O_2 and a series of quantitative microadditions of the test compound. A sample without the test compound was used as the control. The reaction mixtures were incubated at 37 °C for 30 min in a water bath. The absorbance at 520 nm was measured, and the solvent effect was corrected. The scavenging effect for $OH^{\cdot}$ was calculated from the following expression:

$$\text{Scavenging effect}\,\% = (A_{\text{sample}} - A_r)/(A_o - A_r) \times 100\,\%$$

where A_{sample} is the absorbance of the sample in the presence of the test compound, A_r is the absorbance of the blank in the absence of the test compound, and A_o is the absorbance in the absence of the test compound and EDTA-Fe(II) [20].

Synthesis of etobb and bobb

The free ligands etobb and bobb were synthesized according to the literature methods [21–23], as shown in Scheme 1.

Etobb, Yield: 64 %. m. p.: 101–103 °C. ^{1}H NMR (400 MHz, $CDCl_3$,) δ: 7.28 (m, 4H, Ph), 4.12 (s, 2H, CH_2), 4.91 (s, 2H, OCH_2), 1.49 (s, 3H, CH_3). FTIR (KBr ν/cm^{-1}): 756 $\nu_{(O–Ar)}$, 1083 $\nu_{(C–O)}$, 1475 $\nu_{(C=N)}$, 1612 $\nu_{(C=C)}$. UV–Vis (DMF): λ = 280, 288 nm. Anal. Calcd (%): C, 71.8; H, 6.6; N, 16.8; found (%): C, 71.4; H, 6.5; N, 16.6. Λ_M (DMF, 297 K): 0.76 S cm^2 mol^{-1}.

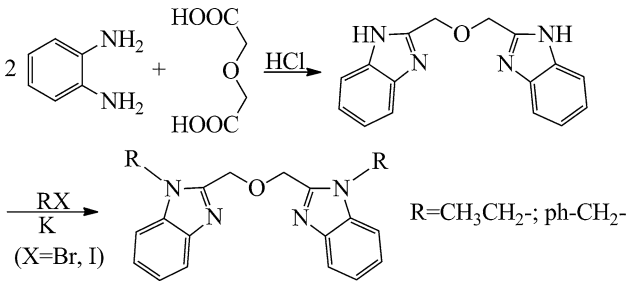

Scheme 1 Synthetic route for ligands, etobb and bobb

Bobb, Yield: 75 %. m. p.: 177–178 °C. ^{1}H NMR ($CDCl_3$–d_1, 400 MHz): δ: 7.78–7.80 (m, 4H), 7.17–7.30 (m, 10H), 6.94–6.96 (m, 4H), 5.29 (s, 4H), 4.80–4.82 (m, 4H). FTIR (KBr ν/cm^{-1}): 1078 $\nu_{(C–O–C)}$, 1496 $\nu_{(C=N)}$, 1463 $\nu_{(C=N–C=C)}$. UV–Vis (DMF): λ = 279, 287 nm. Anal. Calcd (%): C, 78.58; H, 5.71; N, 12.22. found (%): C, 78.51; H, 5.73; N, 12.24. Λ_M (DMF, 297 K): 1.13 S cm^2 mol^{-1}.

Preparation of the complexes

To a stirred solution of sodium crotonate (0.0217 g, 0.20 mmol) in EtOH (5 mL) was added a solution of $AgNO_3$ (0.0340 g, 0.20 mmol) in EtOH (3 mL). A solution of etobb (0.0668 g, 0.20 mmol) in ethanol (5 mL) was then added dropwise. The mixture was vigorously stirred at room temperature for 4 h until the white precipitate had disappeared. The resultant solution was filtered, and a few drops of acetonitrile were added. It was then allowed to evaporate in the dark at room temperature for several days to give colorless block crystals of complex **1**. Complex **2** was prepared by a similar procedure as for complex **1**, using bobb rather than etobb.

Complex **1**, Yield: 69 %. Anal. Calcd for $C_{44}H_{49}AgN_8O_4{\cdot}C_2H_5OH{\cdot}2(CH_3CN){\cdot}2(H_2O)$ (%): C, 58.5; H, 6.4; N, 13.6. Found (%): C, 58.5; H, 6.3; N, 13.7. FTIR (KBr ν/cm^{-1}): 746 $\nu_{(O–Ar)}$, 1043 $\nu_{(C–O)}$, 1558 $\nu_{(C=N)}$. UV–Vis (DMF): λ = 280, 289 nm. Λ_M (DMF, 297 K): 37.1 S cm^2 mol^{-1}.

Complex **2**, Yield: 76 %. Anal. Calcd for $C_{34}H_{31}AgN_4O_3$ (%): C, 62.7; H, 4.8; N, 8.6. Found (%): C, 62.6; H, 4.8; N, 8.7. FTIR (KBr ν/cm^{-1}): 756 $\nu_{(O–Ar)}$, 1066 $\nu_{(C–O)}$, 1556 $\nu_{(C=N)}$. UV–Vis (DMF): λ = 281, 288 nm. Λ_M (DMF, 297 K): 6.6 S cm^2 mol^{-1}.

X-ray crystallography

For each complex, a suitable single crystal was mounted on a glass fiber, and the intensity data were collected on a

Table 1 Crystal data and structure refinement for complexes **1** and **2**

Complex	**1**	**2**
Empirical formula	$C_{50}H_{65}AgN_{10}O_7$	$C_{34}H_{31}AgN_4O_3$
Formula weight	1025.99	651.50
Crystal system	Monoclinic	Triclinic
space group	P21/c	P − 1
a(Å)	15.8523(19)	10.0850(9)
b(Å)	19.987(2)	13.6915(12)
c(Å)	18.7508(15)	14.2747(10)
α(°)	90	71.183(7)
β(°)	116.198(7)	88.486(7)
γ(°)	90	69.361(8)
V(Å^3)	5330.7(9)	1737.5(2)
Z	4	2
ρ_{calcd} (mg m^{-3})	1.278	1.245
μ (mm^{-1})	0.435	0.615
F (000)	2152	668
Crystal size (mm^3)	0.38 × 0.23 × 0.20	0.35 × 0.27 × 0.24
h/*k*/*l* (max, min)	$-18 \le h \le 13$,	$-12 \le h \le 12$,
	$-23 \le k \le 23$,	$-16 \le k \le 15$,
	$-21 \le l \le 22$	$-17 \le l \le 16$
θ range for data collection (°)	1.58–25.00	2.93–25.25
Goodness-of-fit on F^2	1.046	1.040
Final R_1, wR_2 indices ($I > 2\sigma(I)$)	$R_1 = 0.0321$,	$R_1 = 0.0551$,
	$wR_2 = 0.0811$	$wR_2 = 0.1361$
R_1, wR_2 indices (all data)	$R_1 = 0.0445$,	$R_1 = 0.0809$,
	$wR_2 = 0.0916$	$wR_2 = 0.1560$
Largest differences, peak and hole (e Å^{-3})	0.636 and −0.557	0.755 and −0.399

Bruker APEX-II CCD diffractometer with graphite-monochromatized Mo *Kα* radiation ($\lambda = 0.71073$ Å) at 296(2) K. Data reduction and cell refinement were performed using the SAINT suite of programs [24]. The absorption corrections were made by empirical methods. The structures were solved by direct methods and refined by full-matrix least squares against F^2 using SHELXTL software [25]. All H atoms were found in difference electron maps and subsequently refined in a riding model approximation with C–H distances ranging from 0.95 to 0.99 Å and $U_{iso}(H) = 1.2\ U_{eq}(C)$ or $1.5\ U_{eq}(C_{methyl})$. The crystal data and experimental parameters relevant to the structure determination are listed in Table 1. Selected bond distances and angles are given in Table 2.

Results and discussion

Characterization of the complexes

All of these compounds are stable under air. The Ag(I) complexes are soluble in polar aprotic solvents such as DMF and DMSO, slightly soluble in water, methanol, ethanol and acetone, but insoluble in Et_2O and petroleum ether. The elemental analysis shows that their compositions are $[Ag(etobb)_2](crotonate)\cdot C_2H_5OH\cdot 2(CH_3CN)\cdot 2(H_2O)$ and [Ag(crotonate)(bobb)], which were confirmed by the crystal structure analyses. The molar conductance values show that complex **1** is a 1:1 electrolyte, while complex **2** is a non-electrolyte in DMF [26].

The IR spectra of the free ligand etobb and its Ag(I) complex **1** were compared. Free etobb exhibits a characteristic C=N stretching frequency at 1475 cm^{-1}, while the C=N stretching frequency of the complex is observed at 1558 cm^{-1}. Hence, the C=N stretching frequencies are shifted upon complexation [27], indicating that the imine nitrogen atoms are coordinated to the Ag(I) center. Similar shifts are also observed for complex **2**. This deduction agrees with the results of the X-ray crystal structure determinations.

DMF solutions of the free ligands and Ag(I) complexes show, as expected, almost identical UV spectra. Band observed for free etobb at 288 nm is marginally red-shifted in the complex **1** by just 1 nm. The absorption band of

Table 2 Selected bond lengths (Å) and bond angles (°) of complexes **1** and **2**

Complex **1**				
Bond distances	Ag(1)–N(1)	2.292(2)	Ag(1)–N(3)	2.2979(19)
	Ag(1)–N(7)	2.3006(18)	Ag(1)–N(5)	2.3476(19)
Bond angles	N(1)–Ag(1)–N(3)	103.57(7)	N(1)–Ag(1)–N(7)	115.30(7)
	N(3)–Ag(1)–N(7)	117.47(7)	N(1)–Ag(1)–N(5)	110.17(7)
	N(3)–Ag(1)–N(5)	108.70(7)	N(7)–Ag(1)–N(5)	101.55(7)
	C(29)–N(5)–Ag(1)	124.91(16)	C(26)–N(5)–Ag(1)	126.51(15)
	C(19)–N(3)–Ag(1)	128.78(17)	C(16)–N(3)–Ag(1)	125.51(15)
	C(39)–N(7)–Ag(1)	127.06(16)	C(36)–N(7)–Ag(1)	126.27(15)
	C(9)–N(1)–Ag(1)	127.98(17)	C(6)–N(1)–Ag(1)	125.90(16)
Complex **2**				
Bond distances	Ag(1)–N(2)	2.214(4)	Ag(1)–O(2)	2.238(4)
	Ag(1)–N(4)	2.359(4)		
Bond angles	N(2)–Ag(1)–O(2)	143.80(15)	N(2)–Ag(1)–N(4)	105.47(13)
	O(2)–Ag(1)–N(4)	110.35(14)		
	C(21)–N(2)–Ag(1)	126.0(3)	C(22)–N(2)–Ag(1)	128.1(3)
	C(1)–N(4)–Ag(1)	122.6(3)	C(7)–N(4)–Ag(1)	125.0(3)

280 nm in the spectrum of free etobb are assigned to π–π^* (imidazole) transition [28]. Analogously, the UV bands of bobb (279, 287 nm) are also marginally red-shifted by about 1–2 nm in the spectrum of complex **2**.

Crystal structure of complex 1

The asymmetric unit of **1** consists of a $[Ag(etobb)_2]^+$ cation, a crotonate anion, one ethanol molecule, two acetonitrile molecules and two waters of crystallization. As shown in Fig. 1, the Ag(I) atom is four coordinate with a AgN_4 chromophore, provided by four nitrogen atoms from two etobb ligands. The coordination geometry is best described as a distorted tetrahedron. Owing to this coordination geometry, two eight-membered rings are constructed, which are connected through the Ag(I) center.

In complex **1**, the interactions, including π–π interactions and hydrogen bonds, contribute to the formation of a 1D chain and 2D infinite sheet. Similarly, as depicted in Fig. 2, there are two kinds of π–π interactions in complex **1**, between two benzimidazole rings located in the face-to-face position, $d = 3.588(2)$ and 3.618(4) Å. It is precisely such a layout that makes the produces of an infinite 1D zigzag chain. The solvent water molecules and counter anions form strong hydrogen bonds. The hydrogen bonding distances (Å) and angles (°) are listed in Table 3. The 2D layers are linked together by O–H···O and C–H···O hydrogen bonds, as shown in Fig. 3.

Crystal structure of complex 2

Complex **2** has a mononuclear three-coordinate configuration. The structure consists of a central metal Ag(I) atom, plus bobb and crotonate ligands (Fig. 4). The Ag(I) atom is coordinated by one oxygen atom from a crotonate anion and two nitrogen atoms from a bobb ligand. The Ag–O bond distance is 2.238(4) Å, falling into the normal range [29]. Similarly, the units are extended into a 1D supramolecular chain through π–π stacking interactions between benzimidazole rings and weak hydrogen C–H(Benzyl)···O(crotonate) interactions, but these are different to the complex **1**. In complex **1**, π–π stacking is present between each unit [$d = 3.441(4)$ Å], while in complex **2** it is not, as shown in Fig. 5.

The intramolecular distances further reveal the presence of C–H···M close intramolecular interactions between the Ag center and the bobb H(8A) atom (Fig. 5), with an Ag···H distances of 2.818(3) Å, Ag···C distances of 3.377(4) Å (d(Ag···H) < d(Ag···C)) and C–H···Ag angle of 117.498(7)° (C–H···Ag > 100°), which are similar to the values for related Ag(I) complexes [30]. Such C–H···M close interactions can be described as weak intramolecular C–H···M hydrogen bonds; this depiction is also chemically and geometrically reasonable [31–33]. Moreover, from the viewpoint of geometrical requirements, the weak C–H···Ag interactions may facilitate the formation of the coordination bond between Ag(I) and the N-donor atom of the benzimidazole ring in the solid state.

DNA-binding properties

The binding abilities of the free ligand and its metal complexes with CT-DNA were characterized by measuring their effects on the UV–Vis spectra. Compounds binding to DNA through intercalation usually result in hypochromism and bathochromism due to strong π–π stacking interactions

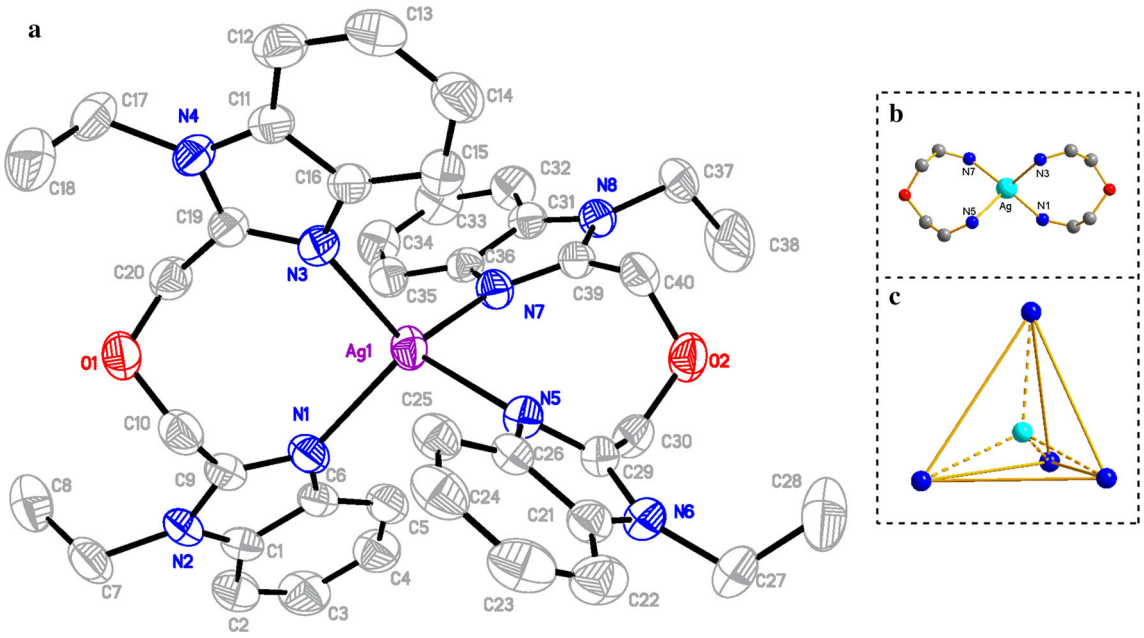

Fig. 1 **a** Molecular structure of the complex **1** with displacement ellipsoids drawn at the 30 % probability level; the solvent molecules and H atoms are omitted. **b** Two eight-membered ring were constructed and connected through the Ag(I) center. **c** Coordination polyhedron of Ag(I)

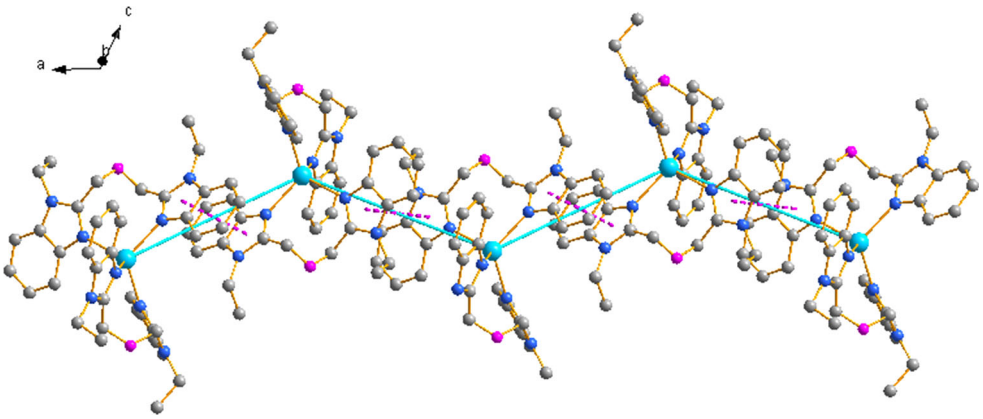

Fig. 2 Structure of the complex **1** linked via π–π stacking interaction (*dashed lines*)

Table 3 Selected hydrogen bonding distances (Å) and angles (°) for complex **1**

D–H···A	*d*(D–H)	*d*(H···A)	*d*(D···A)	∠(DHA)
O(7)–H(3 W)···O(6)#1	0.87	2.11	2.880(5)	146.9
O(6)–H(2 W)···O(4)#1	0.85	1.92	2.766(5)	175.0
O(6)–H(1 W)···O(4)#3	0.85	2.00	2.833(5)	166.3
C(40)–H(40B)···N(5)#1	0.97	2.57	3.244(3)	126.8
C(30)–H(30B)···N(7)#1	0.97	2.57	3.253(3)	127.7
C(23)–H(23)···O(6)#1	0.93	2.51	3.404(4)	160.5
C(40)–H(40A)···O(3)#2	0.97	2.50	3.446(4)	165.8
C(37)–H(37A)···O(3)#2	0.97	2.59	3.522(5)	161.9

Symmetry transformations used to generate equivalent atoms: #1 *x*, *y*, *z*; #2 $-x + 1$, $y - 1/2$, $-z + 1/2$; #3 $-x + 2$, $-y + 1$, $-z + 1$

between the aromatic chromophore and DNA base pairs [34]. It is generally accepted that the extent of hypochromism in the UV–Vis band is consistent with the strength of intercalation [35]; hence, these observations suggest that the compounds interact with CT-DNA by intercalation.

The application of electronic absorption spectroscopy in DNA-binding studies is one of the most useful techniques [36]. To obtain the absorption spectra, the required amount of CT-DNA was added to both the compound and reference solutions to eliminate the absorbance of CT-DNA itself. From the absorption titration data, the binding constant (K_b) was determined using the following equation [37]:

$$[\mathrm{DNA}]/(\varepsilon_a - \varepsilon_f) = [\mathrm{DNA}]/(\varepsilon_b - \varepsilon_f) + 1/K_b(\varepsilon_b - \varepsilon_f)$$

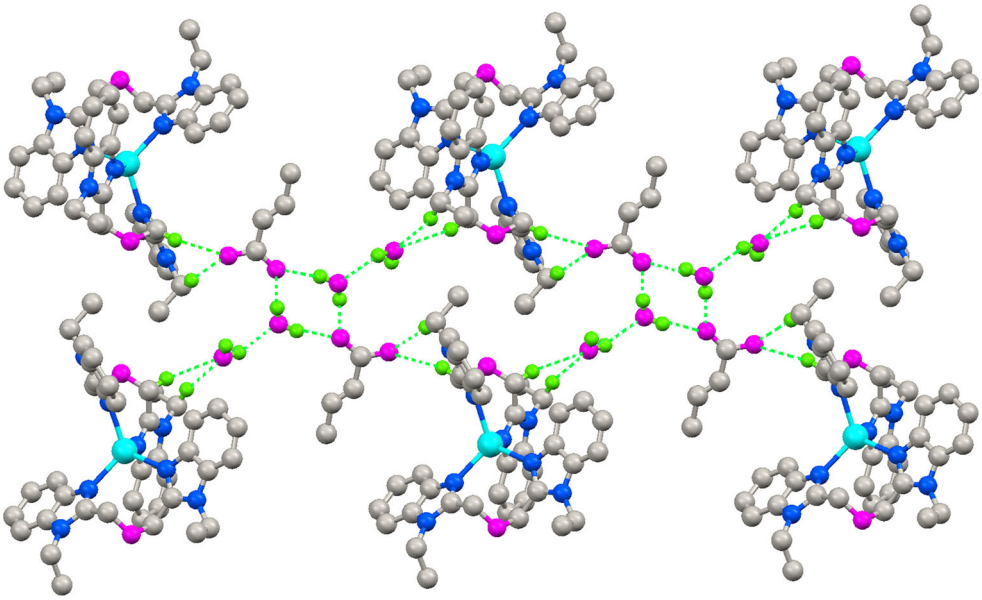

Fig. 3 2D layer generated by hydrogen bonds (*dashed lines*) in complex **1**

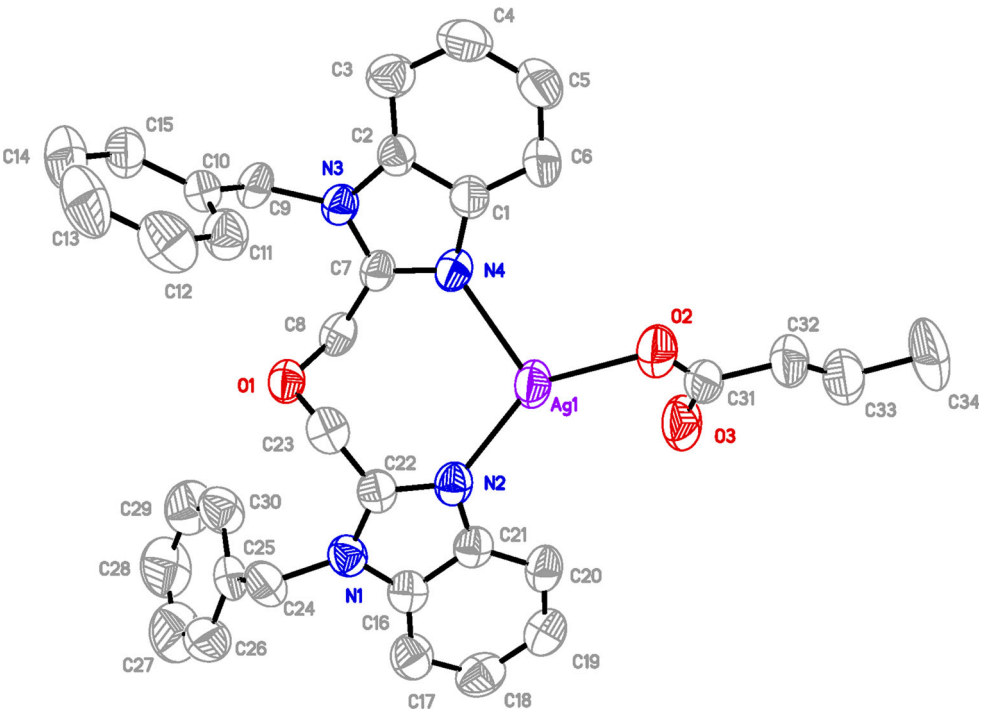

Fig. 4 Environment of the Ag(I) cation in complex **2** showing 30 % thermal probability ellipsoids. The H atoms are omitted

where [DNA] is the concentration of CT-DNA in the base pairs, ε_a corresponds to the observed extinction coefficient (A_{obsd}/[M]), ε_f corresponds to the extinction coefficient of the free compound, ε_b is the extinction coefficient of the complex when fully bound to CT-DNA, and K_b is the intrinsic binding constant. The ratio of slope to intercept in the plot of [DNA]/($\varepsilon_a - \varepsilon_f$) versus [DNA] gave the value of K_b.

The electronic absorption spectra of the two complexes in the absence and presence of CT-DNA are shown in Fig. 6. A band is observed at 270 nm for both complexes **1** and **2**. Upon addition of increasing CT-DNA concentrations, these bands exhibited hypochromism of 49.8 and 49.0 %, respectively. From the electronic absorption spectroscopy experiments, K_b values for complexes **1** and **2** were obtained as 3.88×10^5 and 1.31×10^5 M^{-1}, respectively. The charge transfer of the ligands resulting from coordination of the ligands to the Ag(I) atom should reduce the charge density of the planar conjugate system, which is conducive to intercalation [38].

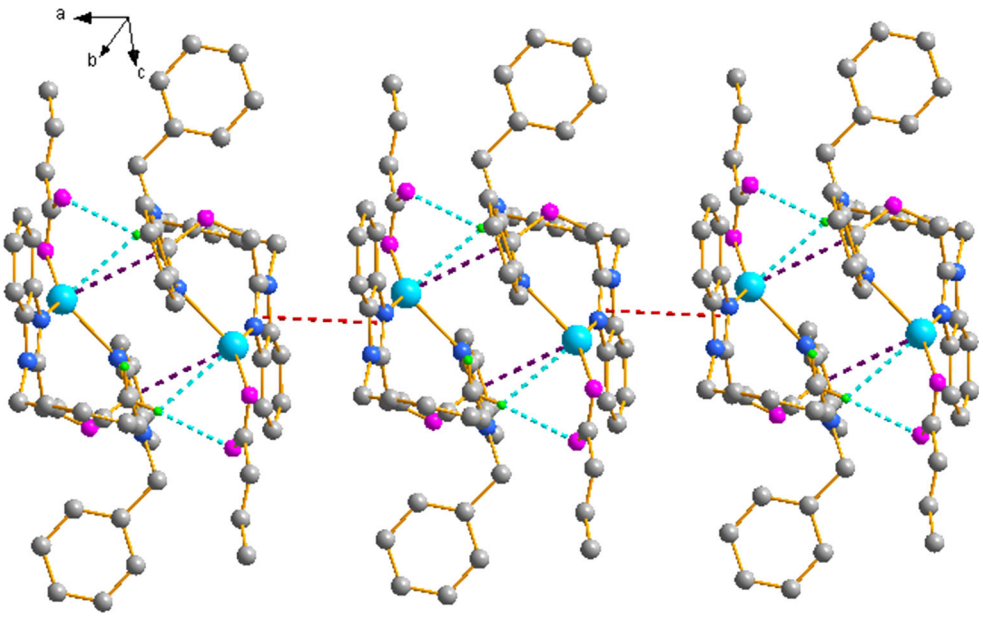

Fig. 5 The 1D supramolecular chain of complex **2** formed via π–π stacking interactions, C–H···O hydrogen bonding interactions and C–H···Ag H-bonding

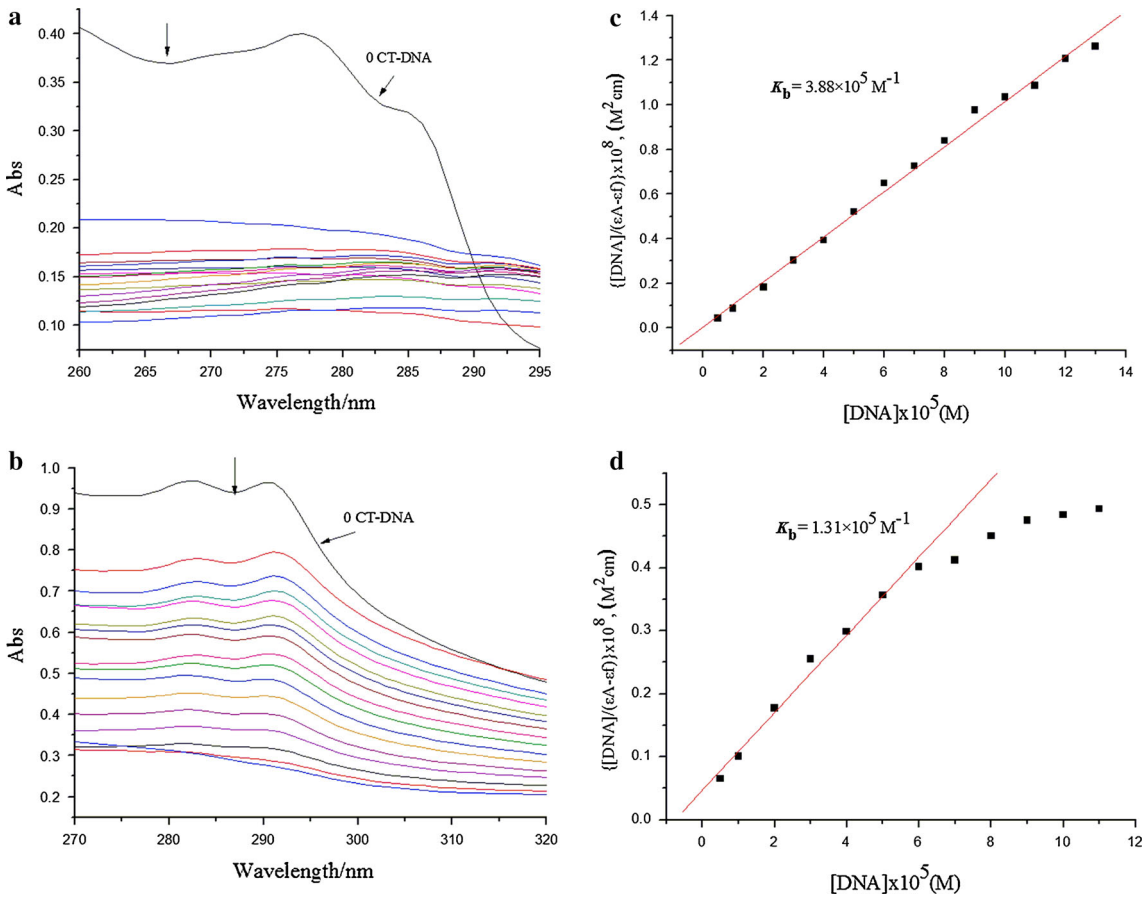

Fig. 6 Electronic spectra of the complex **1** (**a**) and complex **2** (**b**) in Tris–HCl buffer upon addition of CT-DNA. The *arrow* shows the emission intensity changes upon increasing DNA concentrations. [DNA]/($\varepsilon_a - \varepsilon_f$) versus [DNA] for the titration of the complex **1** (**c**) and complex **2** (**d**) with CT-DNA

Next, the DNA binding was investigated by fluorescence spectroscopy. EB does not show any appreciable emission in buffer solution due to fluorescence quenching by the solvent. Upon addition of the ligand or complex to a solution containing EB, no change in the fluorescence spectra was observed. However, the fluorescence intensity of EB is

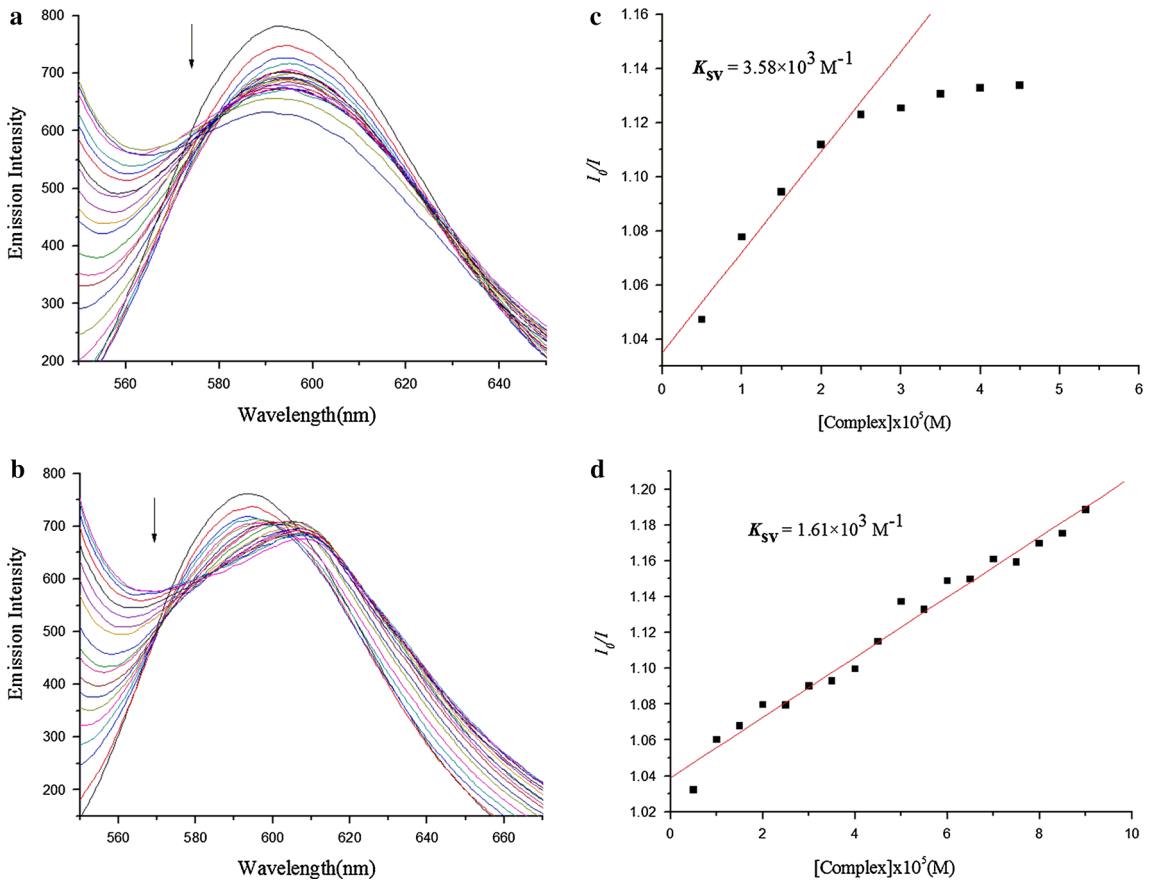

Fig. 7 Emission spectra of EB bound to CT-DNA in the presence of complex **1** (**a**) and complex **2** (**b**), $\lambda_{ex} = 596$ nm. The *arrows* show the intensity changes upon increasing concentrations of the complexes. Fluorescence quenching curves of EB bound to CT-DNA by the complex **1** (**c**) and complex **2** (**d**). [Plots of I_0/I vs. (Complex).]

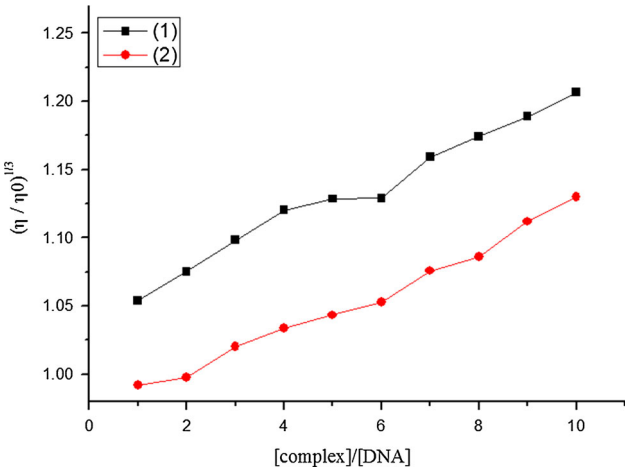

Fig. 8 Effect of increasing amounts of the complexes on the relative viscosity of DNA at 25.0 ± 0.1 °C

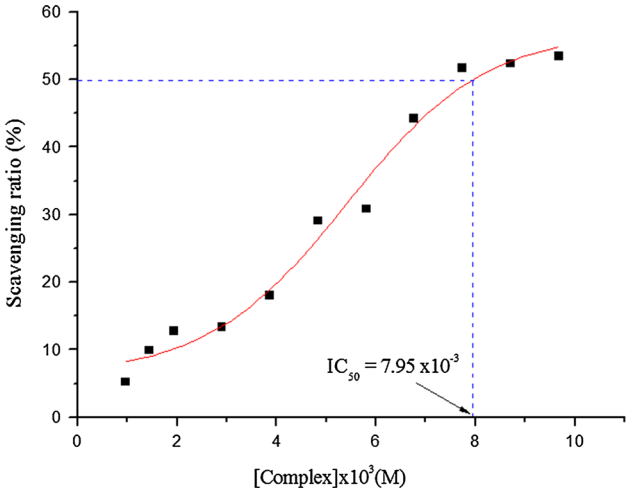

Fig. 9 Plots of hydroxyl radical scavenging effect (%) for the complex **2**

greatly enhanced upon addition of CT-DNA, due to its strong intercalation within the DNA base pairs. Addition of a second molecule, which may bind to DNA more strongly than EB, can result in a decrease in the DNA-induced EB emission by displacement of EB [39]. To further clarify the interaction of the complex with DNA, a competitive binding experiment was carried out in a buffer by keeping

[DNA]/[EB] = 1.13 and varying the concentration of the complex. Fluorescence spectra of EB were measured using an excitation wavelength of 520 nm, and the emission range was set between 550 and 750 nm. The spectra were analyzed according to the classical Stern–Volmer equation [40]:

$$I_0/I = 1 + K_{sv}[Q]$$

where I_0 and I are the fluorescence intensities at 599 nm in the absence and presence of the quencher, respectively, K_{sv} is the linear Stern–Volmer quenching constant, and [Q] is the concentration of the quencher. In these experiments, [CT-DNA] = 2.5×10^{-3} and [EB] = 2.2×10^{-3} mol L^{-1}.

The addition of the compounds results in a significant decrease in the intensity of the emission band of the DNA-EB system at 593 nm, indicating competitive binding of the compounds to DNA. The Stern–Volmer plots (Fig. 7) show that the quenching of EB by the complexes follows a linear relationship, consistent with intercalation of the test compounds. The K_{sv} values for complexes **1** and **2** were 3.58×10^3 and 1.61×10^3 M^{-1}, respectively. Moreover, the binding strengths of the complexes followed the same order as from the UV–Vis experiments.

Hydrodynamic measurements that are sensitive to DNA length changes are regarded as the least ambiguous and most critical test of a binding model in solution in the absence of crystallographic structural data [41, 42]. Viscosity values were calculated from the observed flow times of CT-DNA solutions corrected for the flow time of buffer alone (t_0), $\eta = (t - t_0)$ [43].

As increasing amounts of the complexes were added, the viscosity of the DNA increased steadily. The values of $(\eta/\eta_0)^{1/3}$ were plotted against [compound]/[DNA] (Fig. 8). In classical intercalation, the DNA helix lengthens as base pairs are separated to accommodate the bound ligand, leading to increased DNA viscosity as observed for known intercalators [35], whereas a partial, non-classical ligand intercalation causes a bend (or kink) in the DNA helix, reducing its effective length and therefore its viscosity [19]. Hence, these results provide further evidence that these complexes intercalate with CT-DNA [39] and their DNA-binding affinities follow the order: **1** > **2**. The reason for the different binding affinities can be attributed to differences in steric hindrance and electron density, resulting from the different substituents and geometric structures.

Hydroxyl radical scavenging activity

Figure 9 depicts the inhibitory effect of the compounds on $OH^{\cdot}$ radicals. The inhibitory activity of the compounds is marked, and the suppression ratio increases with increasing concentrations of the test compounds. We compared the present results with those of the well-known natural antioxidants mannitol and vitamin C, using the same method as reported in a previous paper [44, 45]. The 50 % inhibitory concentration (IC_{50}) values of mannitol and vitamin C are ca 9.6×10^{-3} and 8.7×10^{-3} M, respectively. According to the antioxidant experiments, the IC_{50} value of the Ag(I) complex **2** is 7.95×10^{-3} M, which implies that complex **2** is a better scavenger of hydroxyl radicals than both mannitol and vitamin C.

Conclusion

Two Ag(I) complexes with different flexible bis(benzimidazole) ligands and the same crotonate anion have been prepared and characterized through single-crystal X-ray diffraction analyses. These compounds display diverse architectures from 1D to 3D. The results indicate that the bis(benzimidazole) ligands and crotonate ligands both have important effects on structures of the complexes. DNA-binding studies indicate that both complexes bind to DNA via intercalation. Complex **2** can bind to DNA more strongly than complex **1** and also has hydroxyl radical scavenging activity. These results suggest that the Ag(I) complexes could be useful in design of new antitumor drugs.

Supplementary material

Crystallographic data (excluding structure factors) for the structure in this article have been deposited with the Cambridge Crystallographic Data Center as supplementary publication CCDC 1000103 and CCDC 1000104. Copies of the data can be obtained, free of charge, on application to the CCDC, 12 Union Road, Cambridge CB2 1EZ, UK.

Acknowledgments The present research was supported by the National Natural Science Foundation of China (Grant No. 21367017), the Fundamental Research Funds for the Gansu Province Universities (212086), Natural Science Foundation of Gansu Province (Grant No. 1212RJZA037) and 'Qing Lan' Talent Engineering Funds for Lanzhou Jiaotong University.

References

1. Banerjee R, Phan A, Wang B, Knobler C, Furukawa H, O'Keeffe M, Yaghi OM (2008) Science 319:939
2. Lin X, Blake AJ, Wilson C, Sun XZ, Champness NR, George MW, Hubberstey P, Mokaya R, Schroder M (2006) J Am Chem Soc 128:10745
3. Dinca M, Yu AF, Long JR (2006) J Am Chem Soc 128:8904
4. Nouar F, Eubank JF, Bousquet T, Wojtas L, Zaworotko MJ, Eddaoudi M (2008) J Am Chem Soc 130:1833
5. Chen BL, Liang CD, Yang J, Contreras DS, Clancy YL, Lobkovsky EB, Yaghi OM, Dai S (2006) Angew Chem Int Ed 45:1390

6. Fang QR, Zhu GS, Xue M, Wang ZP, Sun JY, Qiu SL (2008) Cryst Growth Des 8:319
7. Ma SQ, Sun DF, Ambrogio M, Fillinger JA, Parkin S, Zhou HC (2007) J Am Chem Soc 129:1858
8. Kaes C, Katz A, Hosseini MW (2000) Chem Rev 100:3553
9. Noro S, Kitaura R, Kondo M, Kitagawa S, Ishii T, Matsuzaka H, Yamashita M (2002) J Am Chem Soc 124:2568
10. Ye BH, Tong ML, Chen XM (2005) Coord Chem Rev 249:545
11. Haque RA, Ghdhayeb MZ, Budagumpi S, Salman AW, Khadeer Ahamed MB, Majid AMSA (2013) Inorg Chim Acta 394:519
12. Fuente T, Martın-Fontecha M, Sallander J, Benhamu B, Campillo M, Medina RA, Pellissier LP, Claeysen S, Dumuis A, Pardo L, Lopez-Rodrıguez ML (2010) J Med Chem 53:1357
13. Dogan O, Demir S, Ozdemir I, Cetinkaya B (2011) Appl Organomet Chem 25:163
14. Beheshti A, Clegg W, Khorramdin R, Nobakht V, Russo L (2011) J Chem Soc Dalton Trans 40:2815
15. Beheshti A, Clegg W, Brooks NR, Sharafi F (2005) Polyhedron 24:435
16. Sanchez-Moreno M, Entrala E, Janssen D, Salas-Peregrin JM, Osuna A (1996) Pharmacology 52:61
17. Yang ZY, Wang Y, Wang Y (2007) Bioorg Med Chem Lett 17:2096
18. Pan GL, Bai YC, Wang H, Kong J, Shi FR, Zhang YH, Wang XL, Wu HL (2013) Z Naturforsch B 68:257
19. Satyanarayana S, Dabroniak JC, Chaires JB (1992) Biochemistry 31:9319
20. Guo ZY, Xue RE, Liu S, Yu HH, Wang PB, Li CP, Li PC (2005) Bioorg Med Chem Lett 15:4600
21. Wu HL, Shi FR, Wang XL, Zhang YH, Bai YC, Kong J, Wang CP (2014) Transition Met Chem 39:261
22. Wu HL, Yun RR, Wang KT, Li K, Huang XC, Sun T, Wang YY (2010) Z Anorg Allg Chem 636:1397
23. Wu HL, Kou F, Jia F, Liu B, Yuan JK, Bai Y (2012) Z Anorg Allg Chem 638:443
24. Bruker (2007) APEX2 and SAINT. Bruker Axs, Inc., Madison
25. Sheldrick GM (1996) SHELXTL. Siemens Analytical X-ray Instruments Inc., Madison
26. Geary WJ (1971) Coord Chem Rev 7:81
27. Dong WK, Sun YX, Liu GH, Li L, Dong XY, Gao XH (2012) Z Anorg Allg Chem 638:1370
28. Thompson LK, Ramaswamy BS, Seymour EA (1977) Can J Chem 55:878
29. Naodovic M, Yamamoto H (2008) Chem Rev 108:3132
30. Sloufovaa I, Sloufb M (2000) Acta Crystallogr Sect C 56:1312
31. Thakur TS, Desiraju GR (2006) Chem Commun (5):552
32. Liu CS, Chen PQ, Yang EC, Tian JL, Bu XH, Li ZM, Sun HW, Lin ZY (2006) Inorg Chem 45:5812
33. Steed JW, Johnson K, Legido C, Junk PC (2003) Polyhedron 22:769
34. Peng B, Chao H, Sun B, Li H, Gao F, Li LN (2006) J Inorg Biochem 100:1487
35. Liu JG, Zhang QL, Shi XF, Ji LN (2001) Inorg Chem 40:5045
36. Wu HL, Gao YC (2004) Trans Met Chem 29:175
37. Xi PX, Xu ZH, Liu XH, Chen FH, Zeng ZZ, Zhang XW, Liu Y (2009) J Fluoresc 19:63
38. Indumathy R, Weyhermüller T, Nair BU (2010) Dalton Trans 39:2087
39. Pasternack RF, Caccam M, Keogh B, Stephenson TA, Williams AP, Gibbs FJ (1991) J Am Chem Soc 113:6835
40. Lakowicz JR, Webber G (1973) Biochemistry 12:4161
41. Mahadevan S, Palaniandavar M (1998) Inorg Chem 37:693
42. Chauhan M, Banerjee K, Arjmand F (2007) Inorg Chem 46:3072
43. Tan CP, Liu J, Chen LM, Shi S, Ji LN (2008) J Inorg Biochem 102:1644
44. Shakir M, Azam M, Ullah MF, Hadi SM (2011) J Photochem Photobiol B 104:449
45. Yellappa S, Seetharamappa J, Rogers LM, Chitta R, Singhal RP, D'Souza F (2006) Bioconjug Chem 17:1418